Article:
Capel Berdiell, I, García-López, V, Howard, MJ et al. (2 more authors) (2021) The Effect of Tether Groups on the Spin States of Iron(II)/Bis[2,6-Di(pyrazol-1-yl)pyridine] Complexes. Dalton Transactions: an international journal of inorganic chemistry. ISSN 1477-9226

https://doi.org/10.1039/D1DT01076J

The Effect of Tether Groups on the Spin States of Iron(II)/*Bis*[2,6-Di(pyrazol-1-yl)pyridine] Complexes†‡

Izar Capel Berdiell,[a,b] Victor García-López,[c] Mark J. Howard,[a] Miguel Clemente-León[c] and Malcolm A. Halcrow*,[a]

The synthesis of six 2,6-di(pyrazol-1-yl)pyridine derivatives bearing dithiolane or carboxylic acid tether groups is described: [2,6-di(pyrazol-1-yl)pyrid-4-yl]methyl (*R*)-lipoate (L^1), 2-[(2,6-di(pyrazol-1-yl)pyridine)-4-carboxamido]ethyl (*R*)-lipoate (L^2), 2-[(2,6-di(pyrazol-1-yl)pyridine)-4-carboxy]ethyl (*R*)-lipoate (L^3), *N*-([2,6-di(pyrazol-1-yl)pyrid-4-ylsulfanyl]-2-aminoethyl (*R*)-lipoamide (L^4), 2-[(2,6-di(pyrazol-1-yl)pyridine)-4-carboxamido]acetic acid (L^5) and 2-[(2,6-di(pyrazol-1-yl)pyridine)-4-carboxamido]propionic acid (L^6). The iron(II) perchlorate complexes of all the new ligands exhibit gradual thermal spin-crossover (SCO) in the solid state above room temperature, except L^4 whose complex remains predominantly high-spin. Crystalline $[Fe(L^6)_2][ClO_4]_2 \cdot 2MeCN$ contains three unique cation sites which alternate within hydrogen-bonded chains, and undergo gradual SCO at different temperatures upon warming. The SCO midpoint temperature ($T_{½}$) of the complexes in CD_3CN solution ranges between 208-274 K, depending on the functional group linking the tether groups to the pyridyl ring. This could be useful for predicting how these complexes might behave when deposited on gold or silica surfaces.

Introduction

Iron(II) complexes of 2,6-di(pyrazolyl)pyridine (bpp) ligands are the largest and most versatile family of compounds for spin-crossover (SCO) research (Scheme 1).[1-3] Over 100 complex salts of $[Fe(bpp)_2]^{2+}$ derivatives are known, around half of which exhibit thermal spin-crossover at accessible temperatures.[4,5] Their popularity stems from the synthetic versatility of the bpp ligand framework, which allows substituents to be appended to the ligand framework using commercially available starting materials, or by simple functional group transformations of pre-formed bpp precursors. Such substituents have a predictable steric and electronic influence on the spin-state of $[Fe(bpp)_2]^{2+}$ derivatives, at least in solution.[6-8] In particular, electron-withdrawing 'R' substituents in Scheme 1 consistently stabilise the low-spin form of the complex, and thus raise the temperature of spin-crossover.[7]

Thus, SCO compounds bearing conducting,[9] fluorescent,[10,11] magnetically active[12,13] and photoswitchable[14,15] functional 'R' substituents have been produced by derivatising the

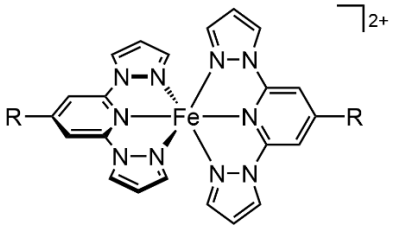

$[Fe(bpp^R)_2]^{2+}$

Scheme 1. The $[Fe(bpp^R)_2]^{2+}$ family of spin-crossover complexes. The parent ligand bpp has R = H.

$[Fe(bpp^R)_2]^{2+}$ core (Scheme 1). Examples bearing long chain alkyl substituents (as potentially mesogenic materials) are also established,[16,17] as are polymetallic complexes,[11,18] coordination polymers[16,19] and metallacycles[15,20] based on ditopic bpp^R derivatives[21]. Finally, tether groups have been appended to bpp^R ligands, with a view to producing switchable (supra)molecular aggregates, self-assembled monolayers or single molecule junctions based on $[Fe(bpp^R)_2]^{2+}$ centres.[13,22-26] To date, however, nanoscience with $[Fe(bpp^R)_2]^{2+}$ derivatives has had mixed success, reflecting that SCO complex molecules often decompose when in contact with conducting surfaces.[27,28]

The high-spin form of iron(II) is much more labile towards ligand exchange reactions than the low-spin form.[29] We reasoned the apparent instability of $[Fe(bpp^R)_2]^{2+}$ centres in surface chemistry might reflect their predominantly high-spin nature under ambient conditions. Published $[Fe(bpp^R)_2]^{2+}$

[a] *School of Chemistry, University of Leeds, Woodhouse Lane, Leeds, UK LS2 9JT. E-mail: m.a.halcrow@leeds.ac.uk.*
[b] *Current address: Institute of Electronic Structure and Laser, Foundation for Research and Technology - Hellas, P.O. Box 1527, GR-711 10 Heraklion, Greece.*
[c] *Instituto de Ciencia Molecular, Universidad de Valencia, Catedrático José Beltrán 2, 46980, Spain.*
‡ Data supporting this study are available at http://doi.org/10.5518/###.
† Electronic Supplementary Information (ESI) available: synthetic procedures and characterisation data for L^1-L^6; crystallographic data, refinement details, Figures and Tables for the ligand and complex structures; and additional solid and solution phase characterisation data. CCDC 2074276−2074283.

derivatives bearing tether substituents linked to the bpp ligand core through amino, alkyl or alkynyl functionalities should have a ≥90 % high-spin state population in solution at room temperature,[7] based on the Hammett parameters of those substituent types.[30] Therefore, alternative linker groups that boost the population of low-spin molecules at room temperature, might be more suited to this kind of surface chemistry by reducing the lability of the deposited complexes. For example, Bousseksou *et al*. have recently used thin films exhibiting SCO above room temperature in a number of prototype devices.[31]

As a first step towards that end, we report six new bpp derivatives bearing alkyldithiolane (lipoate) or alkylcarboxylate tethers, bound to the bpp skeleton *via* different linker groups (*L*^{1}-*L*^{6}, Scheme 2). The spin state properties of their iron complexes in solution were of particular interest, to confirm if the Hammett parameters of the linker functional groups are a reliable guide to their spin states in solution.

Results and Discussion

[2,6-Di(pyrazol-1-yl)pyrid-4-yl]methyl (*R*)-lipoate (*L*^{1}) was synthesised by esterification of 4-(hydroxymethyl)-2,6-di(pyrazol-1-yl)pyridine (bpp^{CH2OH}, Scheme 1)[32] with (*R*)-lipoic acid. The extended tether on 2-[(2,6-di(pyrazol-1-yl)pyridine)-4-carboxamido]ethyl (*R*)-lipoate (*L*^{2}) was prepared from 2,6-di(pyrazol-1-yl)pyridine-4-carboxylic acid (bpp^{CO2H})[33] in four steps (Scheme 3). The linkage isomerism of the ethanolamino function in step (iii) was unexpected, but has some precedent;[34] it proceeds in 60 % yield in a refluxing water:dimethyl sulfoxide solvent mixture. The synthesis of 2-[(2,6-di(pyrazol-1-yl)pyridine)-4-carboxy]ethyl (*R*)-lipoate (*L*^{3}) followed a similar route, but only required two steps. The intermediate 2-[(2,6-di(pyrazol-1-yl)pyridine)-4-carboxy]-2-ethanol was obtained cleanly by treatment of bpp^{CO2H} with ethylene glycol and an acid catalyst, then esterified with (*R*)-lipoic acid as before.

A different approach was taken to *N*-([2,6-di(pyrazol-1-yl)pyrid-4-ylsulfanyl]-2-aminoethyl (*R*)-lipoamide (*L*^{4}). The intermediate [2,6-di(pyrazol-1-yl)pyrid-4-ylsulfanyl]-2-amino-ethane was constructed in one pot by treating 2,4,6-trifluoro-pyridine with BOC-protected 2-aminoethane thiol and 2 equiv. pyrazole using NaH as base (Scheme 4). The yield of this step is moderate at 31 % after deprotection, but the product is readily purified by chromatography. This route is more convenient than using 4-mercapto-2,6-di(pyrazol-1-yl)pyridine (bpp^{SH}, Scheme 1) as a precursor, which must itself be prepared in three steps.[20] Lastly, *L*^{5} and *L*^{6} were prepared by treatment of bpp^{CO2H} with the *tert*butyl ester of the appropriate amino acid, followed by cleavage of the ester group with trifluoroacetic acid.

All of *L*^{1}-*L*^{6} were obtained in NMR and analytical purity, and the identities of *L*^{1}-*L*^{3} were also confirmed crystallographically. While the two unique molecules in the structure of *L*^{1} have extended lipoate chains with all *anti* torsions (Figure S16†), the ethyl lipoate tethers in *L*^{2} and *L*^{3} both have a *gauche* torsion in the XCH_2CH_2O (X = N or O) ethylenyl moiety (Figures 1 and S19†). The structure of *L*^{3} also contains two unique molecules,

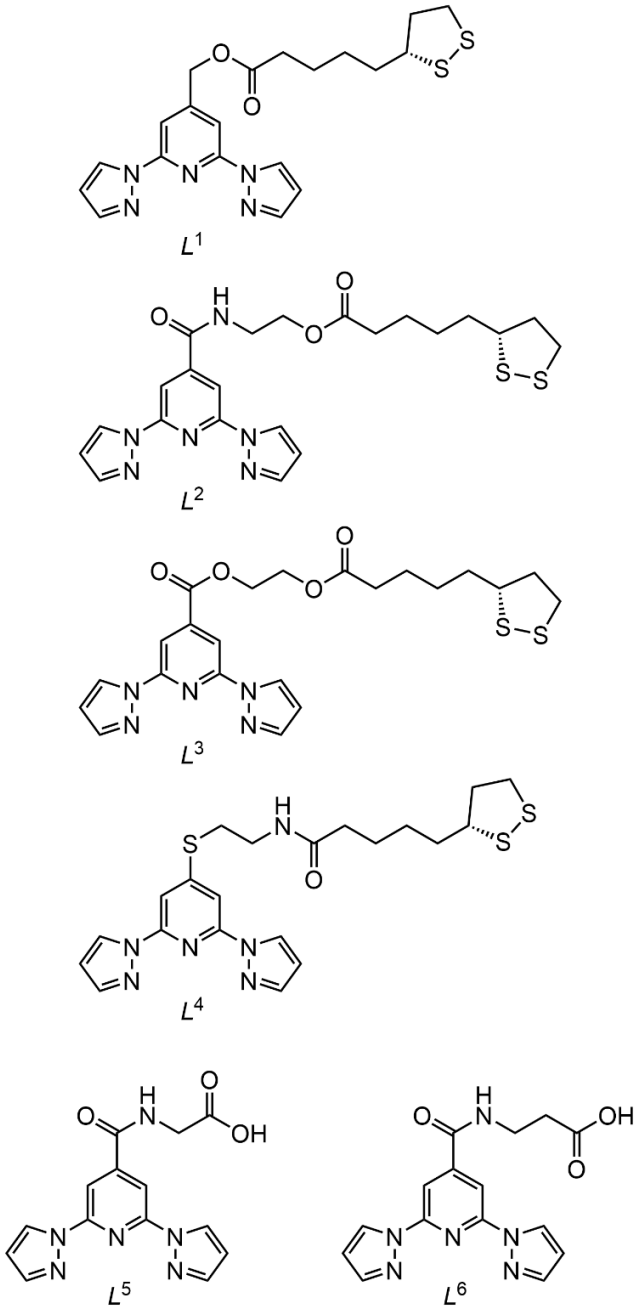

Scheme 2 The bpp derivatives bearing tether groups synthesised in this work.

whose lipoate groups are both highly disordered. That may reflect the lipid bilayer-like molecular packing in that crystal, where the mobile lipoate and rigid heterocyclic domains of the molecules are segregated into bilayers which zig-zag along the (100) plane (Figure 2). *L*^{1} and *L*^{2} do not form lipid bilayer lattices. A crystal structure of *tert*butyl 2-[(2,6-di(pyrazol-1-yl)-pyridine)-4-carboxamido]acetate, the intermediate in the synthesis of *L*^{5}, is also included in the ESI (Figures S21 and S22†).

Complexation of $Fe[ClO_4]_2{\cdot}6H_2O$ with 2 equiv. *L*^{1}-*L*^{6} in acetonitrile at 298 K yields $[FeL_2][ClO_4]_2$ (L = *L*^{1}-*L*^{6}) after the usual work-up. The bright yellow colour of $[Fe(L^4)_2][ClO_4]_2$ indicates it is high-spin in the solid state at room temperature, whereas the other complexes have the orange or red colouration consistent

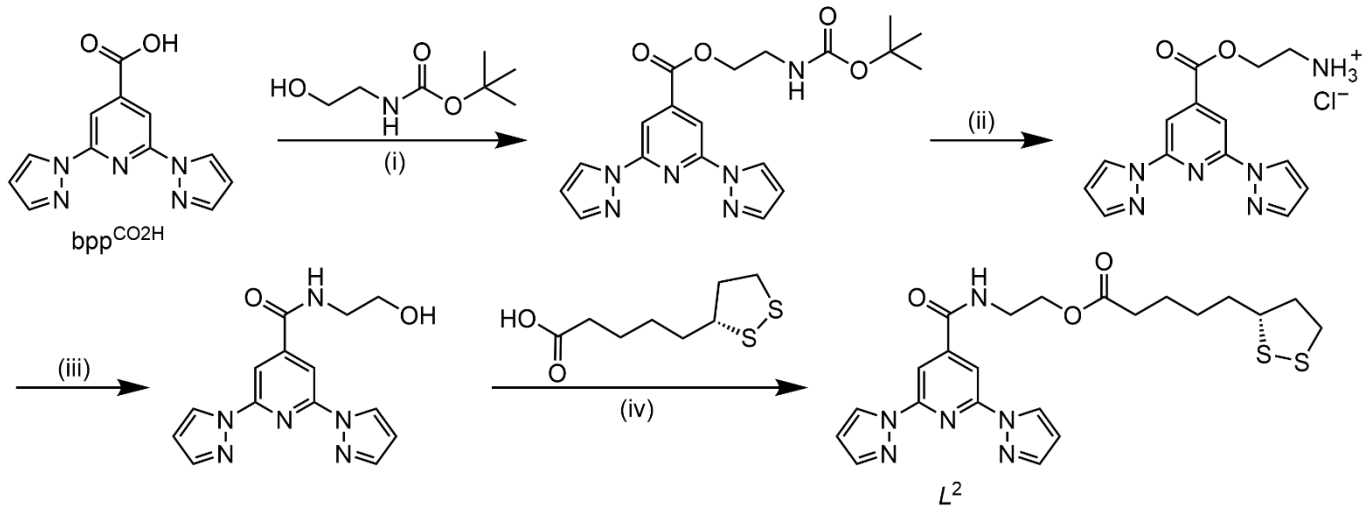

Scheme 3 Synthesis of L^2. Reagents and conditions: (i) 4-dimethylaminopyridine, *N*,*N*-dicyclo-hexyl carbodiimide, dichloromethane, 0 °→room temperature→reflux; (ii) acyl chloride, methanol, 0 °→room temperature; (iii) water, dmso, reflux then Na_2CO_3, room temperature; (iv) 4-dimethylaminopyridine, *N*,*N*-dicyclohexyl carbodiimide, dichloromethane, 0 °→ room temperature.

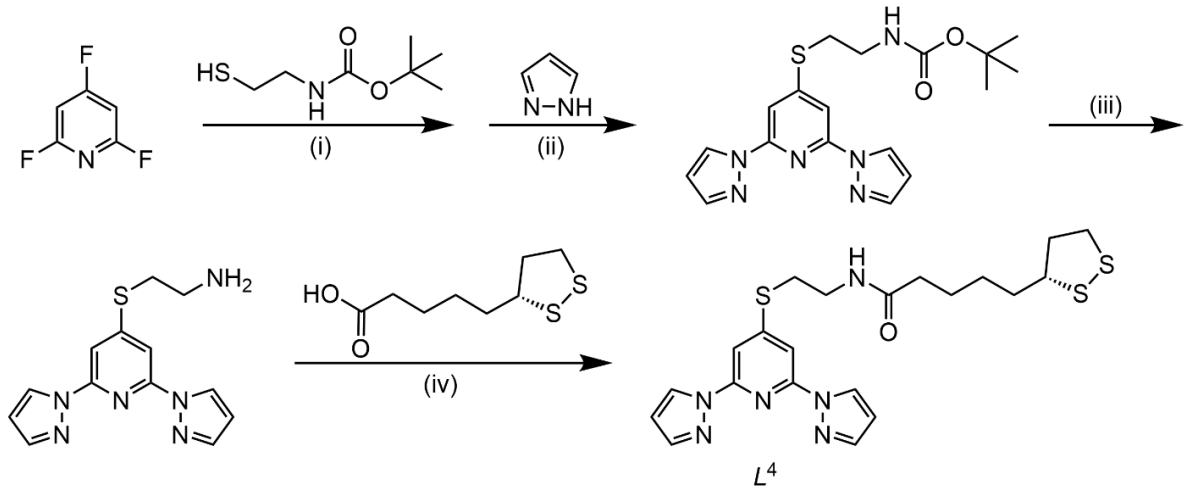

Scheme 4 Synthesis of L^4. Reagents and conditions: (i) NaH, thf, room temperature; (ii) NaH, thf, room temperature, then water; (iii) acyl chloride, methanol, 0 °→room temperature then water, Na_2CO_3; (iv) 4-dimethylaminopyridine, *N*,*N*-dicyclohexyl carbodiimide, dichloromethane, 0 °→ room temperature.

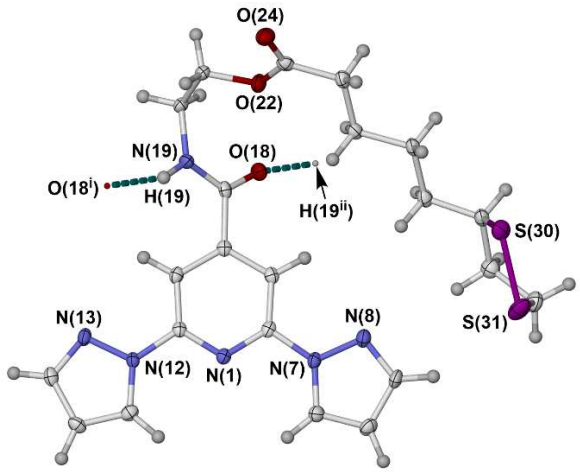

Figure 1 The asymmetric unit in the crystal of L^2. Displacement ellipsoids are at the 50 % probability level except H atoms which have arbitrary radii. Colour code: C, white; H, pale grey; N, blue; O, red; S, purple. Symmetry codes: (i) 1+*x*, *y*, *z*; (ii) −1+*x*, *y*, *z*.

with a mixed spin-state population.[4] None of the lipoate-containing complexes were characterised crystallographically, but structures were obtained from acetonitrile solvates of $[Fe(L^5)_2][ClO_4]_2$ and $[Fe(L^6)_2][ClO_4]_2$.

Crystallisation of $[Fe(L^5)_2][ClO_4]_2$ from acetonitrile/diethyl ether yielded two crystal morphologies, plates (monoclinic, $P2_1/n$, Z = 4) and needles (triclinic, $P\bar{1}$, Z = 2). Monoclinic $[Fe(L^5)_2][ClO_4]_2$·MeCN was the major form in the crystallisation vials, and was fully characterised. However, triclinic $[Fe(L^5)_2][ClO_4]_2$·*x*MeCN ($x \approx 1.5$) diffracted weakly and was highly disordered, so only a preliminary structure solution of that solvate was possible (Figure S26†). Both crystals are low-spin at 120 K according to their metric parameters, which is conveniently expressed by the volume of the FeN_6 coordination octahedron in the complexes (V_{Oh}, Tables 1 and S3†).[35] High-spin and low-spin $[Fe(bpp^R)_2]^{2+}$ derivatives typically show $V_{Oh} \geq 11.5$ and < 10 Å^3, respectively.[36]

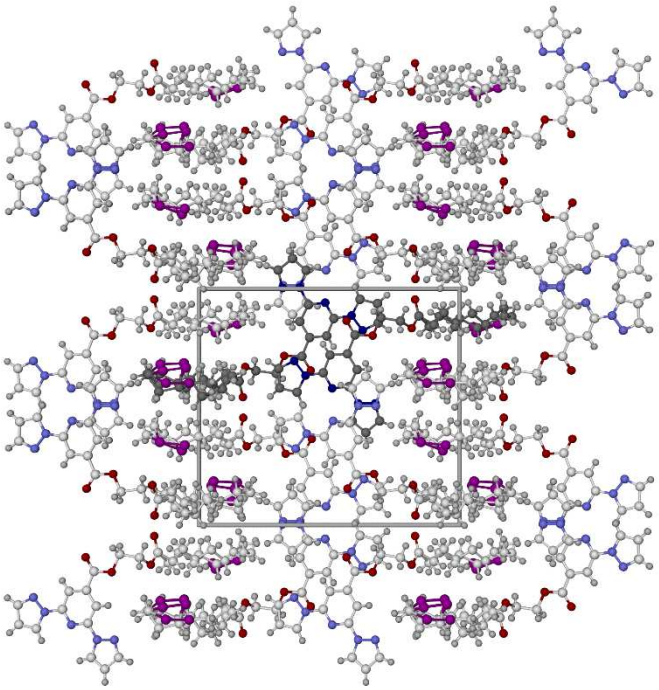

Figure 2 The lipid bilayer crystal packing in L^3, showing the crystallographic unit cell. The view is parallel to the [100] crystal vector, with *c* horizontal. All orientations of the disordered lipoate residues are included, and one molecule from each environment in the asymmetric unit is highlighted with dark colouration. Colour code: C, white or dark grey; H, pale grey; N, pale or dark blue; O, red; S, purple.

Table 1 Octahedral coordination volumes (V_{Oh}, Å^3) for the crystallographically characterised complexes in this work.

	120 K	High temperature[a]
$[Fe(L^5)_2][ClO_4]_2$·MeCN	9.665(10)	11.375(17)
$[Fe(L^6)_2][ClO_4]_2$·2MeCN:		
molecule A	9.506(10)	9.595(17)
molecule B	9.802(10)	11.30(2)
molecule C	9.620(8)	10.443(15)

[a]This is 330 K for $[Fe(L^5)_2][ClO_4]_2$·MeCN, and 290 K for $[Fe(L^6)_2][ClO_4]_2$·2MeCN.

Crystals of $[Fe(L^5)_2][ClO_4]_2$·MeCN contain one unique cation environment, which associates into zig-zag chains along the *n* glide plane *via* an intermolecular O–H···O hydrogen bond between their carboxylic acid groups. These chains are linked into layers in the (100) plane with a 4^4 hydrogen-bond topology,[37] by two N–H···O interactions to a bridging ClO_4^- ion (Figure 3). The hydrogen-bonded layers associate weakly into three dimensions through face-to-face $\pi\cdots\pi$ contacts, between two pyrazolyl rings on each cation molecule.

The complex is low-spin at 120 K (Table 1), and has the usual near-regular D_{2d}-symmetric coordination geometry for a low-spin complex of this type. However a second structure determination at 330 K showed the compound has transformed to a predominantly high-spin form. There is little change in the angular coordination geometry between the temperatures, showing the SCO involves a simple expansion of the Fe–N bonds without any other rearrangement of the ligands. That is consistent with a gradual SCO on warming, as observed in the magnetic data (see below).[38,39] The 330 K structure also has more pronounced anion disorder, and librational disorder of a carboxamido group whose O atom is in contact with one of the anions. There is no sign of reduced occupancy of the MeCN solvent molecule at the higher temperature however, implying SCO in the crystal is not connected to solvent loss.[8,40]

Crystals of $[Fe(L^6)_2][ClO_4]_2$·2MeCN (triclinic, $P\bar{1}$, $Z = 6$) have a homogeneous morphology, and an asymmetric unit containing three formula units of the compound. The three unique cations are essentially low-spin at 120 K, although the values for V_{Oh} and other structural parameters shown by molecule B are at the upper end of what is expected for a low-spin complex (Tables 1 and S6†).[4,36,41] Hence, that cation site could contain a small population of high-spin molecules. Otherwise, the only significant structural difference between the cations is a slight twisting of the heterocyclic ligand donors in molecule C. This is evidenced by the dihedral angle between the least squares planes of the two heterocyclic ligand cores (θ),[42] which should be 90° in an idealised $[Fe(bpp^R)_2]^{2+}$ species. Molecules A, B and C in this structure exhibit θ = 88.78(3), 89.38(4) and 85.35(3)° respectively (Table S6†). These values are all in the usual range for low-spin $[Fe(bpp^R)_2]^{2+}$ salts, however.[4,41]

Besides their slightly different molecular geometries, the cation sites are distinguished by the pattern of intermolecular hydrogen bonding in the lattice. The cations are linked into 1D chains along the $[51\bar{1}]$ crystal vector, by $R_2^2(8)$ pairs of O–H···O hydrogen bonds between their carboxylic acid groups (Figure 4).[43] The three cation environments are disposed in an ABCABC arrangement within these chains. The hydrogen bonded chains in turn form layers in the (011) plane through three N–H···O hydrogen bonds between carboxamido groups in cations of type B and A, C and A, and two C molecules. The other

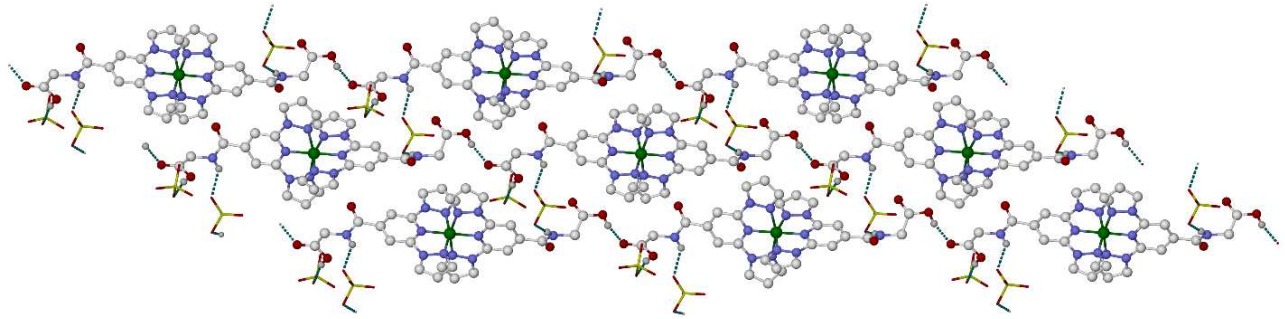

Figure 3 A hydrogen-bonded cation layer in $[Fe(L^5)_2][ClO_4]_2$·MeCN at 120 K. Only one orientation of the disordered anions is included, which are de-emphasised for clarity. C-bound H atoms, and residues that do not contribute to hydrogen bonding, are omitted from the view. Colour code: C, white; H, pale grey; Cl, yellow; N, blue; O, red.

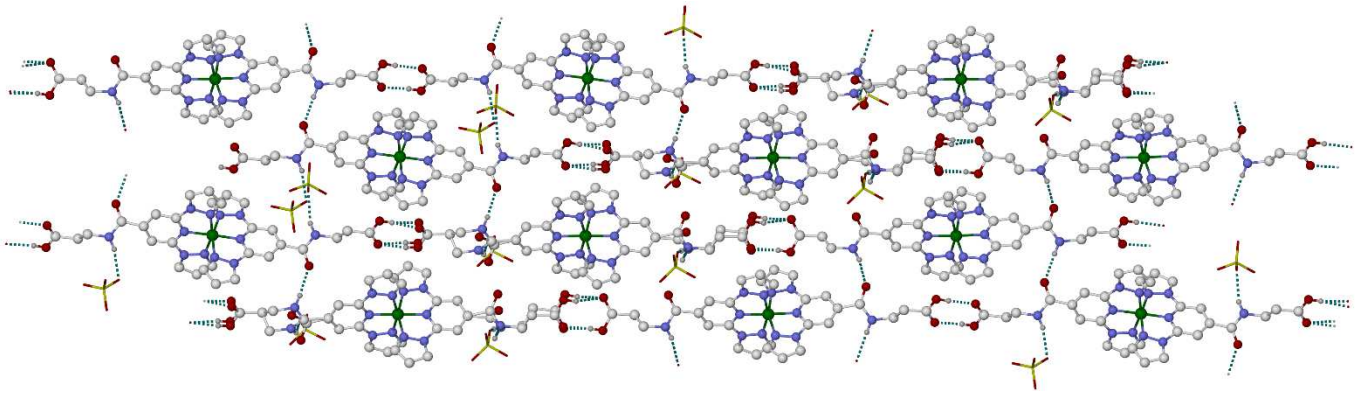

Figure 4 A hydrogen-bonded cation layer in $[Fe(L^6)_2][ClO_4]_2 \cdot 2MeCN$ at 120 K, highlighting the chains of cations linked by $R_2^2(8)$ hydrogen bonds between their carboxylic acid substituents. Each horizontal cation chain in the view contains one 'A', one 'B' and one 'C' molecular environment. Both disorder orientations of the carboxamidopropionic acid substituents in molecule B are included in the view. Other details as for Figure 3.

carboxamido N–H groups in the asymmetric unit donate hydrogen bonds to different perchlorate ions. Topologically speaking, molecules A, B and C are connected to 4, 3 and 5 nearest neighbours respectively by these interactions. The resultant 2D hydrogen bond network has topology $(4{\cdot}3{\cdot}4{\cdot}5)(4{\cdot}5^2)(3{\cdot}4{\cdot}3{\cdot}5^2)$ in the short Schläfli notation,[37] which is derived from a simpler 6,4-connected network by deletion of one connection (Figure S28†). A minor conformational disorder orientation in the carboxamidopropionic acid substituents of molecule B reduces its hydrogen bond connectivity from 3 to 2, but does not otherwise affect this description. There are three unique, short intermolecular face-to-face $\pi\cdots\pi$ interactions at 120 K between cations in the lattice, including one between molecule A and its inversion symmetry equivalent which associates the hydrogen-bonded 2D sheets into centrosymmetric bilayers (Figure S29†).

A second structure determination at 290 K was obtained from the same crystal. While the crystallographic symmetry has not changed, the three cation environments have different spin-state populations: molecule A is still low-spin; molecule B is predominantly high-spin; and molecule C has a mixed spin-state population (Table 1). This corresponds to a *ca.* 40 % overall high-spin population in the crystal at this temperature. As before, there is little change in the coordination geometries of molecules B and C beyond their expanded Fe–N bonds. SCO at molecule B is accompanied by an increased libration in its propionic acid side chains, although attempts to treat these with a disorder model were unsuccessful. More disorder is evident in the lattice at 290 K, which could not be modelled because the crystal diffracted too weakly at room temperature. However, there is again no evidence for solvent loss from the crystal at the higher temperature.

The different tendencies of molecules A-C to undergo thermal SCO on warming, B > C > A, cannot be easily attributed to their molecular geometries.[41] The small θ distortion in molecule C could have stabilised the high-spin form of that cation site, other things being equal, but that isn't observed in practise.[41,42] The relevance of their slightly different low-spin Fe–N bond lengths is also unclear, without the fully high-spin structure for comparison.[41] The intermolecular environment about each cation site was examined with a Hirshfeld analysis.[44] This did not identify any gross differences between the intermolecular contacts to the three cations, which could explain their different spin state properties (Figures S31-S36†). However, two weak intermolecular contacts to the pyrazolyl donor groups of molecule A are positioned to restrict the expansion of those Fe–N{pyrazolyl} bonds, which could trap that molecule in its low-spin state. First is a C–H···C contact between C(10A) and a MeCN methyl group C(80), which is 0.2 Å shorter in the Hirshfeld map for the room temperature structure [C(10)···C(80) = 4.089(6) Å at 290K; Figure S34†]. Second is the previously mentioned centrosymmetric close contact and $\pi\cdots\pi$ interaction between the pyrazolyl groups of two 'A' molecules, which would require those molecules to expand against each other if SCO took place (Figures S29 and S30†). There is also a comparable contact between nearest neighbour 'C' molecules, but their corresponding interatomic distances are 0.2-0.4 Å longer than for the 'A' cation pair.

Most of the complexes exhibit gradual and incomplete SCO equilibria from magnetic susceptibility data, with mixed high: low-spin populations at room temperature and a significant residual high-spin fraction at low temperatures (Figure S39†). Such gradual SCO is often found in poorly crystalline materials with heterogeneous molecular environments; and, in compounds containing flexible ligand substituents, which act as inert spacers between switching centres in the lattice. In some cases, the incomplete transitions may reflect thermal trapping of a fraction of the samples in their high-spin state on cooling below 100 K.[45,46] That is common in $[Fe(bpp)_2]^{2+}$ derivatives whose SCO extends below that temperature.[15,18,20,46,47] In other cases the onset of SCO occurs at high temperatures, implying these samples might be structurally heterogeneous with a mixture of SCO-active and high-spin iron sites. That is also consistent with the poor crystallinity of many of the complexes.

A sample of the monoclinic pseudopolymorph of $[Fe(L^5)_2][ClO_4]_2$ was isolated by a Pasteur separation for the magnetic susceptibility measurements (Figure S37†). SCO in this compound, which has the shortest tether group substituent, occurs less gradually than for the other materials with a midpoint ($T_{½}$) near room temperature (Figure S39†). That is to be expected from the crystal structure of this solvate, which is low-spin at 120 K but essentially high-spin at 330K (Table 1).

However, samples of $[Fe(L^6)_2][ClO_4]_2$ exhibit $T_{½}$ > 350 K and are only *ca.* 25 % high-spin at room temperature, which is less than predicted crystallographically. That may reflect structural changes following solvent loss from the sample.

The exception to this behaviour is $[Fe(L^4)_2][ClO_4]_2$, which is high-spin at 300 K and shows an unusual $\chi_M T$ *vs* *T* profile on cooling (Figure S39†). A decrease from $\chi_M T$ = 3.5 to 3.0 cm³ mol⁻¹ K between 250-100 K is consistent with a typically gradual SCO in *ca.* 15 % of the sample. However, $\chi_M T$ then recovers to 3.5 cm³ mol⁻¹ K upon further cooling to 50 K, an apparent "reverse SCO". Reverse-SCO events are rare, being entropically disfavoured, but similar low temperature behaviour has been seen in some other SCO compounds bearing flexible alkyl substituents.[48]

The spin states of the complexes in solution should be a better guide to their behaviour when deposited on surfaces. Hence, the SCO equilibria for five of the compounds in CD_3CN solution were determined by Evans method (Figure 5). The errors on these data are relatively large, because of the complexes' moderate solubility and high molecular weight. None-the-less, $T_{½}$ values for the complexes of ligands bearing carboxy and carboxamido tether group linkers (L^2, L^3 and L^5) are identical within experimental error, and are higher than the other compounds (Table 2). The data agree with our previous correlation of $T_{½}$ with the pyridyl 'R' substituents in $[Fe(bpp^R)_2]^{2+}$ derivatives, where the comparison can be made (Figure S40†).[7] This confirms the SCO properties of $[Fe(bpp^R)_2]^{2+}$ complexes bearing tether groups or other 'R' substituents can be predicted from the electronic properties of the functional group linking the tether to the ligand core.

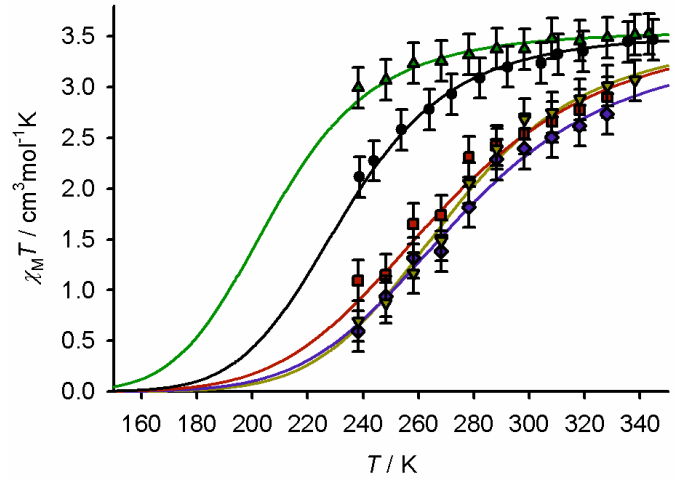

Figure 5 Magnetic susceptibility data in CD_3CN solution for: $[Fe(L^1)_2][ClO_4]_2$ (black ●), $[Fe(L^2)_2][ClO_4]_2$ (red ■), $[Fe(L^3)_2][ClO_4]_2$ (blue ◆), $[Fe(L^4)_2][ClO_4]_2$ (green ▲) and $[Fe(L^5)_2][ClO_4]_2$ (yellow ▼). The lines show the best fit of the data to a thermodynamic SCO equilibrium (eq 1 and 2, Experimental Section).

Conclusion

Six new bpp^R derivatives bearing lipoate (dithiolane) or carboxylic acid 'R' tether groups of varying chain lengths have been prepared, which might be suitable for deposition onto gold/semiconductor, or oxide/silica, surfaces. Iron(II) perchlorate complexes of the lipoate ligand derivatives L^1-L^4 are poorly crystalline and were not structurally characterised, but solvates of $[Fe(L^5)_2][ClO_4]_2$ and $[Fe(L^6)_2][ClO_4]_2$ were analysed crystallographically.

Table 2 SCO data for four of the complexes in this work in CD_3CN solution (Figure 5). Typical thermodynamic values for SCO in $[Fe(bpp^R)_2]^{2+}$ derivatives can be found in ref. 7.

	$T_{½}$, K	ΔH, kJ mol⁻¹	ΔS, J mol⁻¹ K⁻¹
$[Fe(L^1)_2][ClO_4]_2$	234(2)	−22.9(11)	98.1
$[Fe(L^2)_2][ClO_4]_2$	269(3)	−19.4(13)	72.3
$[Fe(L^3)_2][ClO_4]_2$	275(2)	−21.2(10)	77.3
$[Fe(L^4)_2][ClO_4]_2$	208(5)	−19.3(16)	92.7
$[Fe(L^5)_2][ClO_4]_2$	271(1)	−23.9(8)	85.6

Unusually, $[Fe(L^6)_2][ClO_4]_2{\cdot}2MeCN$ crystallises as linear hydrogen-bonded chains of three unique iron centres, alternating in ABCABC fashion. The 'A', 'B' and 'C' iron sites undergo gradual thermal SCO at different temperatures, as evidenced by its room temperature crystal structure. Its gradual SCO contrasts with $[Fe(bpp^{CO2H})_2]X_2$ (Scheme 1, R = CO_2H; X^- = BF_4^- or ClO_4^-), which also crystallise in linear chains of $R_2^2(8)$ hydrogen-bonded cations but show abrupt spin-transitions with narrow thermal hysteresis.[49] The flexible $C(O)NHC_2H_4$ spacers between the $[Fe(bpp)_2]^{2+}$ switching centres and the carboxylic hydrogen bonding groups in $[Fe(L^6)_2][ClO_4]_2$ should contribute to its lower SCO cooperativity compared to $[Fe(bpp^{CO2H})_2]X_2$, where those groups are directly linked.

Solution magnetic data appear to confirm our proposal that the spin states of $[Fe(bpp^R)_2]^{2+}$ complexes bearing tether groups can be predicted, from the properties of the substituent linking the tether to the bpp^R ligand core (Figure 5). The $[FeL_2][ClO_4]_2$ complexes bearing carboxy or carboxamido ligand groups (L = L^2, L^3 and L^5) clearly show undergo SCO *ca.* 35 K higher than the complex with an alkoxyalkyl linker (L = L^1), and *ca.* 65 K higher than the complex with an alkylsulfanyl linker (L = L^4). These data agree with our previous correlation between $T_{½}$ and σ_P and σ_P^+ Hammett parameters of the $[Fe(bpp^R)_2]^{2+}$ 'R' substituent (although the analysis is hindered by the unavailability of σ_P^+ values for some substituents; Figure S40†).[7]

Figure 5 shows the low-spin fractions of $[FeL_2][ClO_4]_2$ in CD_3CN at 298 K are zero for L = L^4, which is fully high-spin; 8 % for L = L^1; and 30 ±2 % for L = L^2, L^3 and L^5. A $[Fe(bpp^R)_2]^{2+}$ derivative must probably be at least 50 % low-spin at room temperature, before the kinetic inertness of the low-spin state influences its stability in a surface monolayer. That could be achieved, for example, by modifying L^2, L^3, L^5 or L^6 with electron-donating pyrazolyl substituents which also predictably raise $T_{½}$.[7] Experiments towards that end are in progress.

Experimental

Synthetic protocols and characterisation data for L^1-L^6 are given in the ESI†.

CAUTION Although we have experienced no problems when using the perchlorate salts in this study, metal-organic perchlorates are potentially explosive and should be handled with care in small quantities.

Syntheses of $[Fe\boldsymbol{L}_2][ClO_4]_2$ ($\boldsymbol{L}$ = $\boldsymbol{L}^1$-$\boldsymbol{L}^6$). The same procedure, as described here for $[Fe(L^1)_2][ClO_4]_2$, was used for all the complexes bearing tether substituents. A mixture of $Fe[ClO_4]_2{\cdot}6H_2O$ (0.085 g, 0.23 mmol) and L^1 (0.20 g, 0.47 mmol) in acetonitrile (10 cm^3) was stirred until all the solid had dissolved. The dark yellow solution was concentrated to *ca.* 5 cm^3 volume and filtered. Slow diffusion of diethyl ether vapor into the solution yielded a yellow powder.

The other complexes were obtained by the same procedure, using equivalent quantities of the appropriate bpp derivative ligand. Yields ranged from 53-78 %.

For $[Fe(L^1)_2][ClO_4]_2$: yellow powder. Found C, 43.0; H, 4.00; N, 12.5 %. Calcd for $C_{40}H_{46}Cl_2FeN_{10}O_{12}S_4$ C, 43.1; H, 4.16; N, 12.6 %. ES-MS *m/z* 457.0996 (calcd for $[Fe(L^3)_2]^{2+}$ 457.0968), 584.0063 (calcd for $[Fe(L^3)ClO_4]^+$ 584.0128), 1013.1337 (calcd for $[Fe(L^3)_2ClO_4]^+$ 1013.1421). ^{1}H NMR (CD_3CN) δ 1.36 (s, 4H), 1.57 (s, 8H), 1.83 (s, 2H), 2.41 (s, 6H), 3.07 (s, 4H – all lipoate CH_2), 3.51 (m, 2H, lipoate C*H*), 8.81 (s, 4H, CH_2O), 38.7, 40.0 (both br s, 4H, pz H^4 and H^5), 60.1, 67.6 (both br s, 4H, pz H^3 and py $H^{3/5}$) ppm.

For $[Fe(L^2)_2][ClO_4]_2$: orange powder. Found C, 42.9; H, 4.20; N, 13.5 %. Calcd for $C_{44}H_{52}Cl_2FeN_{12}O_{14}S_4$ C, 43.0; H, 4.27; N, 13.7 %. ES-MS *m/z* 514.1157 (calcd for $[Fe(L^4)_2]^{2+}$ 514.1183), 641.0307 (calcd for $[Fe(L^4)ClO_4]^{2+}$ 641.0342), 757.1921 (calcd for $[Fe(L^4)_3]^{2+}$ 757.1936). ^{1}H NMR ({CD_3}$_2$CO) δ 1.45 (s, 4H), 1.63 (s, 8H), 1.84 (s, 2H), 2.38 (s, 6H), 3.06 (s, 4H – all lipoate CH_2), 3.55 (s, 2H, lipoate C*H*), 3.80 (s, 4H, CH_2NH), 4.35 (s, 4H, CH_2O), 8.48 (s, 2H, N*H*), 27.7, 30.8 (both br s, 4H, pz H^4 and H^5), 45.1, 48.3 (both br s, 4H, pz H^3 and py $H^{3/5}$) ppm.

For $[Fe(L^3)_2][ClO_4]_2$: this complex formed large orange crystals, which unfortunately diffracted too weakly for crystallographic characterisation. Found C, 43.1; H, 3.90; N, 11.4 %. Calcd for $C_{44}H_{50}Cl_2FeN_{10}O_{16}S_4$ C, 43.0; H, 4.10; N, 11.4 %. ES-MS *m/z* 515.1043 (calcd for $[Fe(L^5)_2]^{2+}$ 515.1023), 758.6696 (calcd for $[Fe(L^5)_3]^{2+}$ 758.6697). ^{1}H NMR (CD_3CN) δ 1.44 (s, 4H), 1.56 (s, 8H), 1.78 (s, 2H), 3.03 (s, 6H), 3.50 (m, 4H – all lipoate CH_2), 3.66 (s, 2H, lipoate C*H*), 4.65, 4.78 (both s, 4H, CH_2O), 22.9, 26.4 (both br s, 4H, pz H^4 and H^5), 39.1, 41.6, (both br s, 4H, pz H^3 and py $H^{3/5}$) ppm.

For $[Fe(L^4)_2][ClO_4]_2$: yellow powder. Found C, 41.8; H, 4.20; N, 13.7 %. Calcd for $C_{42}H_{52}Cl_2FeN_{12}O_{10}S_6$ C, 41.9; H, 4.35; N, 14.0 %. ES-MS *m/z* 502.1018 (calcd for $[Fe(L^6)_2]^{2+}$ 502.1005), 1103.1481 (calcd for $[Fe(L^6)_2ClO_4]^+$ 1103.1495). ^{1}H NMR ({CD_3}$_2$CO) δ 1.15 (s, 4H), 1.41 (s, 4H), 2.15 (s, 4H), 1.67 (s, 6H), 2.42 (m, 2H), 2.78 (s, 4H – all lipoate CH_2), 3.10 (m, 4H, CH_2NH), 3.57 (s, 2H, lipoate C*H*), 4.91 (s, 4H, CH_2S), 7.71 (s, 2H, N*H*), 44.2, 45.4 (both br s, 4H, pz H^4 and H^5), 61.6, 73.4 (both br s, 4H, pz H^3 and py $H^{3/5}$) ppm.

For $[Fe(L^5)_2][ClO_4]_2$: the complex formed red single crystals in a mixture of needle and plate morphologies, which decomposed to a powder on drying. Found C, 38.0; H, 2.70; N, 19.1 %. Calcd for $C_{28}H_{24}Cl_2FeN_{12}O_{14}$ C, 38.3; H, 2.75; N, 19.1 %. ES-MS *m/z* 313.1054 (calcd for $[HL^7]^+$ 313.1044), 340.0662 (calcd for $[Fe(L^7)_2]^{2+}$ 340.0646), 679.1210 (calcd for $[Fe(L^7)_2{-}H]^+$ 679.1213), 779.0752 (calcd for $[Fe(L^7)_2ClO_4]^+$ 779.0776), 991.2175 (calcd for $[Fe(L^7)_3{-}H]^+$ 991.2184). ^{1}H NMR (CD_3CN) δ 4.29 (s, 4H, CH_2), 8.06 (s, 2H, N*H*), 9.87 (br s, 2H, CO_2H), 27.2, 30.9 (both br s, 4H, pz H^4 and H^5), 46.2, 49.7 (both br s, 4H, pz H^3 and py $H^{3/5}$) ppm.

For $[Fe(L^6)_2][ClO_4]_2$: red single crystals, which decomposed to a powder on drying. Found C, 39.6; H, 3.00; N, 18.3 %. Calcd for $C_{30}H_{28}Cl_2FeN_{12}O_{14}$ C, 39.7; H, 3.11; N, 18.5 %. ES-MS *m/z* 327.1201 (calcd for $[HL^8]^+$ 327.1200), 354.0806 (calcd for $[Fe(L^8)_2]^{2+}$ 354.0802), 707.1519 (calcd for $[Fe(L^8)_2{-}H]^+$ 707.1526), 807.1070 (calcd for $[Fe(L^8)_2ClO_4]^+$ 807.1089). ^{1}H NMR (CD_3CN) δ 2.75 (s, 4H, CH_2CO_2), 3.79 (s, 4H, CH_2NH), 7.72 (s, 2H, N*H*), 9.38 (br s, 2H, CO_2H), 29.1, 32.4 (both br s, 4H, pz H^4 and H^5), 48.6, 52.5 (both br s, 4H, pz H^3 and py $H^{3/5}$) ppm.

Single Crystal Structure Analyses

Diffraction data for L^3, whose crystals show weak diffraction arising from extensive disorder, were recorded at station I19 of the Diamond synchrotron (λ = 0.6889 Å). Other crystallographic data were measured with an Agilent Supernova dual-source diffractometer using monochromated Cu-K_α (λ = 1.5418 Å) radiation. The diffractometer was fitted with an Oxford Cryostream low-temperature device. All the structures were solved by direct methods *(SHELXS*[50]), and developed by full least-squares refinement on F^2 (*SHELXL-2018*[50]). Crystallographic figures were prepared using *XSEED*,[51] and octahedral coordination volumes (V_{Oh}) and other structural parameters were calculated with *Olex2*.[52] Hirshfeld surfaces and interaction maps were produced using *CrystalExplorer*.[53]

Experimental details for the structure are listed in Tables S1 and S2†, while details of the crystallographic refinements are also given in the ESI†.

Other measurements

Elemental microanalyses were performed by the microanalytical service at the London Metropolitan University School of Human Sciences. Electrospray mass spectra were recorded on a Bruker MicroTOF-q instrument, from chloroform solution (organic compounds) or nitromethane solution (metal complexes). Any sodium-containing species in the mass spectra originate from the sodium formate calibrant used. Diamagnetic NMR spectra employed a Bruker AV3HD spectrometer operating at 400.1 MHz (^{1}H) or 100.6 MHz (^{13}C), while paramagnetic ^{1}H NMR spectra were obtained with a Bruker AV3 spectrometer operating at 300.1 MHz. X-ray powder diffraction patterns were measured using a Bruker D2 Phaser diffractometer.

Solid state magnetic susceptibility measurements were performed on a Quantum Design MPMS-3 magnetometer, with an applied field of 5000 G and a scan rate of 5 $Kmin^{-1}$. A diamagnetic correction for the sample was estimated from Pascal's constants;[54] a diamagnetic correction for the sample holder was also applied. Magnetic measurements in solution were obtained by Evans method using a JEOL ECA600ii or a Bruker AV500 spectrometer, operating at 500.13 and 600.05 MHz (^{1}H) respectively.[55] A diamagnetic correction for the sample,[54] and a correction for the variation of the density of the solvent with temperature,[56] were applied to these data. The parameters in Table 2 were derived by fitting these data to eq (1) and (2):

$$\ln[(1 - n_{HS}(T))/ n_{HS}(T)] = \Delta H/RT - \Delta S/R \quad (1)$$

$$\Delta S = \Delta H/T_{½} \quad (2)$$

Conflicts of interest

There are no conflicts to declare

Acknowledgements

This work was funded by the Leverhulme Trust (RPG-2015-095) and the Royal Society of Chemistry (RM1602-2118). We thank Diamond Light Source for access to beamline I19 (MT20570), which contributed to the results presented here; O. Cespedes (School of Physics and Astronomy, University of Leeds) for help with the solid-state magnetic measurements; and N. Shahid (School of Chemistry, University of Leeds) for assistance during the preparation of the manuscript.

Notes and references

1 P. Gütlich and H. A. Goodwin (eds), *Spin Crossover in Transition Metal Compounds I–III, Top. Curr. Chem.* vols. **233–235**, Springer, New York, 2004; M. A. Halcrow (ed), *Spin-crossover materials – properties and applications,* John Wiley & Sons, Chichester, UK, 2013, p. 568.

2 J. Zarembowitch, F. Varret, A. Hauser, J. A. Real and K. Boukheddaden, *C. R. Chimie*, 2018, **21**, 1056.

3 K. S. Kumar and M. Ruben, *Coord. Chem. Rev.*, 2017, **346**, 176; S. Rat, M. Piedrahita-Bello, L. Salmon, G. Molnár, P. Demont and A. Bousseksou, *Adv. Mater.*, *2*018, **30**, 1703862; E. Coronado, *Nature Rev. Mater.*, 2020, **5**, 87.

4 M. A. Halcrow, *Coord. Chem. Rev.*, 2009, **253**, 2493; L. J. Kershaw Cook, R. Mohammed, G. Sherborne, T. D. Roberts, S. Alvarez and M. A. Halcrow, *Coord. Chem. Rev.*, 2015, **289–290**, 2.

5 J. Olguin and S. Brooker, *Coord. Chem. Rev.*, 2011, **255**, 203.

6 J. M. Holland, S. A. Barrett, C. A. Kilner and M. A. Halcrow, *Inorg. Chem. Commun.*, 2002, **5**, 328; R. J. Deeth, M. A. Halcrow, L. J. Kershaw Cook and P. R. Raithby, *Chem. Eur. J.*, 2018, **24**, 5204.

7 L. J. Kershaw Cook, R. Kulmaczewski, R. Mohammed, S. Dudley, S. A. Barrett, M. A. Little, R. J. Deeth and M. A. Halcrow, *Angew. Chem. Int. Ed.*, 2016, **55**, 4327.

8 R. Kulmaczewski, M. J. Howard and M. A. Halcrow, *Dalton Trans.*, 2021, **50**, 3464.

9 M. Nihei, N. Takahashi, H. Nishikawa, H. Oshio, *Dalton Trans.*, 2011, **40**, 2154.

10 R. González-Prieto, B. Fleury, F. Schramm, G. Zoppellaro, R. Chandrasekar, O. Fuhr, S. Lebedkin, M. Kappes and M. Ruben, *Dalton Trans.*, 2011, **40**, 7564; A. Santoro, L. J. Kershaw Cook, R. Kulmaczewski, S. A. Barrett, O. Cespedes and M. A. Halcrow, *Inorg. Chem.*, 2015, **54**, 682; K. S. Kumar, I. Šalitroš, N. Suryadevara, E. Moreno-Pineda and M. Ruben, *Eur. J. Inorg. Chem.*, 2018, 5091.

11 B. Schäfer, T. Bauer, I. Faus, J. A. Wolny, F. Dahms, O. Fuhr, S. Lebedkin, H.-C. Wille, Kai Schlage, K. Chevalier, F. Rupp, R. Diller, V. Schünemann, M. M. Kappes and M. Ruben, *Dalton Trans,*. 2017, **46**, 2289.

12 A. Abhervé, M. Palacios-Corella, J. M. Clemente-Juan, R. Marx, P. Neugebauer, J. van Slageren, M. Clemente-León, E. Coronado, *J. Mater. Chem. C*, 2015, **3**, 7936.

13 A. Abhervé, M. J. Recio-Carretero, M. López-Jordà, J. M. Clemente-Juan, J. Canet-Ferrer, A. Cantarero, M. Clemente-León, E. Coronado, *Inorg. Chem.*, 2016, **55**, 9361.

14 K. Takahashi, Y. Hasegawa, R. Sakamoto, M. Nishikawa, S. Kume, E. Nishibori and H. Nishihara, *Inorg. Chem.*, 2012, **51**, 5188.

15 I. Šalitroš, R. Herchel, O. Fuhr, R. González-Prieto and M. Ruben, *Inorg. Chem.*, 2019, **58**, 4310.

16 S. Basak, P. Hui and R. Chandrasekar, *Chem. Mater.*, 2013, **25**, 3408; A. K. Botcha, S. Basak and R. Chandrasekar, *RSC Adv.*, 2014, **4**, 34760; K. S. Kumar, I. Šalitroš, B. Heinrich, S. Moldovan, M. Mauro and M. Ruben, *J. Phys.: Condens. Matter*, 2020, **32**, 204002.

17 I. Galadzhun, R. Kulmaczewski, O. Cespedes, M. Yamada, N. Yoshinari, T. Konno and M. A. Halcrow, *Inorg. Chem.*, 2018, **57**, 13761; I. Galadzhun, R. Kulmaczewski, N. Shahid, O. Cespedes, M. J. Howard and M. A. Halcrow, *Chem. Commun.*, 2021, **57**, 4039.

18 C. A. Tovee, C. A. Kilner, S. A. Barrett, J. A. Thomas and M. A. Halcrow, *Eur. J. Inorg. Chem.*, 2010, 1007.

19 C. Rajadurai, O. Fuhr, R. Kruk, M. Ghafari, H. Hahn and M. Ruben, *Chem. Commun.*, 2007, 2636.

20 L. J. Kershaw Cook, J. Fisher, L. P. Harding and M. A. Halcrow, *Dalton Trans.*, 2015, **44**, 9417.

21 M. Attwood and S. S. Turner, *Coord. Chem. Rev.*, 2017, **353**, 247.

22 D. Secker, S. Wagner, S. Ballmann, R. Härtle, M. Thoss and H. B. Weber, *Phys. Rev. Lett.*, 2011, **106**, 136807; V. Meded, A. Bagrets, K. Fink, R. Chandrasekar, M. Ruben, F. Evers, A. Bernand-Mantel, J. S. Seldenthuis, A. Beukman and H. S. J. van der Zandt, *Phys. Rev. B*, 2011, **83**, 245415.

23 M. S. Alam, M. Stocker, K. Gieb, P. Müller, M. Haryono, K. Student and A. Grohmann, *Angew. Chem. Int. Ed.*, 2010, **49**, 1159; L. Pukenas, F. Benn, E. Lovell, A. Santoro, L. J. Kershaw Cook, M. A. Halcrow and S. D. Evans, *J. Mater. Chem. C*, 2015, **3**, 7890.

24 E. J. Devid, P. N. Martinho, M. V. Kamalakar, I. Šalitroš, Ú. Prendergast, J.-F. Dayen, V. Meded, T. Lemma, R. González-Prieto, F. Evers, T. E. Keyes, M. Ruben, B. Doudin and S. J. van der Molen, *ACS Nano*, 2015, **9**, 4496.

25 K. S. Kumar, I. Šalitroš, Z. Boubegtiten-Fezoua, S. Moldovan, P. Hellwig and M. Ruben, *Dalton Trans.*, 2018, **47**, 35; K. S. Kumar, I. Šalitroš, N. Suryadevara, E. Moreno-Pineda and M. Ruben, *Eur. J. Inorg. Chem.*, 2018, 5091; E. Burzurí, A. García-Fuente, V. García-Suárez, K. S. Kumar, M. Ruben, J. Ferrer and H. S. J. van der Zant, *Nanoscale*, 2018, **10**, 7905.

26 M. Palacios-Corella, J. Ramos-Soriano, M. Souto, D. Ananias, J. Calbo, E. Ortí, B. M. Illescas, M. Clemente-Leon, N. Martín and E. Coronado, *Chem. Sci.*, 2021, **12**, 757.

27 M. Gruber and R. Berndt, *Magnetochemistry*, 2020, **6**, 35; K. S. Kumar and M. Ruben, *Angew. Chem. Int. Ed.*, 2021, **60**, 7502.

28 For other SCO molecules, or different types of spin state-switch, bearing surface tether groups see *eg* G. Poneti, L. Poggini, M. Mannini, B. Cortigiani, L. Sorace, E. Otero, P. Sainctavit, A. Magnani, R. Sessoli and A. Dei, *Chem. Sci.*, 2015, **6**, 2268; G. D. Harzmann, R. Frisenda, H. S. J. van der Zant and M. Mayor, *Angew. Chem. Int. Ed.*, 2015, **54**, 13425; R. Frisenda, G. D. Harzmann, J. A. Celis Gil, J. M. Thijssen, M. Mayor and H. S. J. van der Zant, *Nano Lett.*, 2016, **16**, 4733; H. L. C. Feltham, K. Dankhoff, C. J. Meledandri and S. Brooker, *ChemPlusChem*, 2018, **83**, 582.

29 M. A. Halcrow, *Dalton Trans.*, 2020, **49**, 15560.

30 C. Hansch, A. Leo and R. W. Taft, *Chem. Rev.*, 1991, **91**, 165.

31 M. D. Manrique-Juarez, F. Mathieu, V. Shalabaeva, J. Cacheux, S. Rat, L. Nicu, T. Leïchlé, L. Salmon, G. Molnár and A. Bousseksou, *Angew. Chem. Int. Ed.*, 2017, **56**, 8074; K. Ridier, Y. Zhang, M. Piedrahita-Bello, C. M. Quintero, L. Salmon, G. Molnár, C. Bergaud and A. Bousseksou, *Adv. Mater.*, 2020, **32**, 2000987; Y. Zhang, K. Ridier, V. Shalabaeva, I. Séguy, S. Pelloquin, H. Camon, S. Calvez, L. Routaboul, L. Salmon, G. Molnár and A. Bousseksou, *J. Mater. Chem. C*, 2020, **8**, 8007.

32 J. Elhaïk, C. M. Pask, C. A. Kilner and M. A. Halcrow, *Tetrahedron*, 2007, **63**, 291.
33 T. Vermonden, D. Branowska, A. T. M. Marcelis and E. J. R. Sudhölter, *Tetrahedron*, 2003, **59**, 5039; C. Klein, E. Baranoff, M. Grätzel and M. K. Nazeeruddin, *Tetrahedron Lett.*, 2011, **52**, 584; N. Bridonneau, L. Rigamonti, G. Poneti, D. Pinkowicz, A. Forni and A. Cornia, *Dalton Trans.*, 2017, **46**, 4075.
34 See *eg* M. F. Moreau, D. Godeneche, J. C. Madelmont, G. Meyniel and J. L. Chabard, *Eur. J. Med. Chem.*, 1982, **17**, 557; N. Caldwell, P. S. Campbell, C. Jamieson, F. Potjewyd, I. Simpson and A. J. B. Watson, *J. Org. Chem.*, 2014, **79**, 9347; A. Murre, K. Erkman, S. Kaabel, I. Jarving and T. Kanger, *Synthesis*, 2019, **51**, 4183.
35 P. Guionneau, M. Marchivie, G. Bravic, J.-F. Létard and D. Chasseau, *Top. Curr. Chem.*, 2004, **234**, 97.
36 I. Capel Berdiell, R. Kulmaczewski and M. A. Halcrow, *Inorg. Chem.*, 2017, **56**, 8817.
37 L. Öhrström and K. Larsson, *Molecule-Based Materials – the Structural Network Approach*, Elsevier, Amsterdam, 2005, p. 314.
38 M. A. Halcrow, *Chem. Soc. Rev.*, 2011, **40**, 4119.
39 Abrupt and/or hysteretic spin-transitions in $[Fe(bpp^R)_2]^{2+}$ salts are often accompanied by angular displacement of the bpp^R ligands around the iron atom between the spin states. See *eg* L. J. Kershaw Cook, F. L. Thorp-Greenwood, T. P. Comyn, O. Cespedes, G. Chastanet and M. A. Halcrow, *Inorg. Chem.*, 2015, **54**, 6319; K. S. Kumar, B. Heinrich, S. Vela, E. Moreno-Pineda, C. Bailly and M. Ruben, *Dalton Trans.*, 2019, **48**, 3825.
40 See *eg* Y. Garcia, P. J. Van Koningsbruggen, E. Codjovi, R. Lapouyade, O. Kahn and L. Rabardel, *J. Mater. Chem.*, 1997, **7**, 857; S. Hayami, Z.-Z. Gu, H. Yoshiki, A. Fujishima and O. Sato, *J. Am. Chem. Soc.*, 2001, **123**, 11644; C. Faulmann, K. Jacob, S. Dorbes, S. Lampert, I. Malfant, M.-L. Doublet, L. Valade and J. A. Real, *Inorg. Chem.*, 2007, **46**, 8548; M. Clemente-León, E. Coronado, M. C. Giménez-López and F. M. Romero, *Inorg. Chem.*, 2007, **46**, 11266; J. J. M. Amoore, S. M. Neville, B. Moubaraki, S. S. Iremonger, K. S. Murray, J.-F. Létard and C. J. Kepert, *Chem. Eur. J.*, 2010, **16**, 1973; T. D. Roberts, F. Tuna, T. L. Malkin, C. A. Kilner and M. A. Halcrow, *Chem. Sci.*, 2012, **3**, 349; A. Lennartson, P. Southon, N. F. Sciortino, C. J. Kepert, C. Frandsen, S. Mørup, S. Piligkos and C. J. McKenzie, *Chem. Eur. J.*, 2015, **21**, 16066; W. Phonsri, C. G. Davies, G. N. L. Jameson, B. Moubaraki and K. S. Murray, *Chem. Eur. J.*, 2016, **22**, 1322.
41 M. A. Halcrow, I. Capel Berdiell, C. M. Pask and R. Kulmaczewski, *Inorg. Chem.*, 2019, **58**, 9811.
42 J. M. Holland, J. A. McAllister, C. A. Kilner, M. Thornton-Pett, A. J. Bridgeman and M. A. Halcrow, *J. Chem. Soc., Dalton Trans.*, 2002, 548.
43 M. C. Etter, *Acc. Chem. Res.*, 1990, **23**, 120.
44 J. J. McKinnon, M. A. Spackman and A. S. Mitchell, *Acta Crystallogr., Sect. B: Struct. Sci.*, 2004, **60**, 627; J. J. McKinnon, D. Jayatilaka and M. A. Spackman, *Chem. Commun.*, 2007, 3814; M. A. Spackman and D. Jayatilaka, *CrystEngComm*, 2009, **11**, 19.
45 See eg G. Ritter, E. König, W. Irler and H. A. Goodwin, *Inorg. Chem.*, 1978, **17**, 224; Y. Garcia, V. Ksenofontov, S. Mentior, M. Dirtu, C. Gieck, A. Bhatthacharjee and P. Gütlich, *Chem. Eur. J.*, 2008, **14**, 3745; J.-F. Létard, S. Asthana, H. J. Shepherd, P. Guionneau, A. E. Goeta, N. Suemura, R. Ishikawa and S. Kaizaki, *Chem. Eur. J.*, 2012, **18**, 5924; N. Paradis, G. Chastanet, F. Varret and J.-F. Létard *Eur. J. Inorg. Chem.* 2013, 968; Y. S. Ye, X. Q. Chen, Y. D. Cai, B. Fei, P. Dechambenoit, M. Rouzières, C. Mathonière, R. Clérac and X. Bao, *Angew. Chem. Int. Ed.*, 2019, **58**, 18888; M. Książek, M. Weselski, M. Kaźmierczak, A. Tołoczko, M. Siczek, P. Durlak, J. A. Wolny, V. Schünemann, J. Kusz and R. Bronisz, *Chem. Eur. J.*, 2020, **26**, 14419.
46 V. A. Money, C. Carbonera, J. Elhaïk, M. A. Halcrow, J. A. K. Howard and J.-F. Létard, *Chem. Eur. J.*, 2007, **13**, 5503.
47 See *eg* I. Šalitroš, O. Fuhr and M. Ruben, *Materials*, 2016, **9**, 585; R. Kulmaczewski, E. Trzop, L. J. Kershaw Cook, E. Collet, G. Chastanet and M. A. Halcrow, *Chem. Commun.*, 2017, **53**, 13268; S. Kuramochi, T. Shiga, J. M. Cameron, G. N. Newton and H. Oshio, *Inorganics*, 2017, **5**, 48.
48 R. Akiyoshi, R. Ohtani, L. F. Lindoy and S. Hayami, *Dalton Trans.*, *Dalton Trans.*, 2021, **50**, 5065.
49 A. Abhervé, M. Clemente-León, E. Coronado, C. J. Gómez-García and M. López-Jordà, *Dalton Trans.*, 2014, **43**, 9406; V. García-López, M. Palacios-Corella, A. Abhervé, I. Pellicer-Carreño, C. Desplanches, M. Clemente-León and E. Coronado, *Dalton Trans.*, 2018, **47**, 16958.
50 G. M. Sheldrick, *Acta Cryst. Sect. C.: Struct. Chem.*, 2015, **71**, 3.
51 L. J. Barbour, *J. Supramol. Chem.*, 2001, **1**, 189.
52 O. V. Dolomanov, L. J. Bourhis, R. J. Gildea, J. A. K. Howard and H. Puschmann, *J. Appl. Cryst.*, 2009, **42**, 339.
53 M. J. Turner, J. J. McKinnon, S. K. Wolff, D. J. Grimwood, P. R. Spackman, D. Jayatilaka and M. A. Spackman, *CrystalExplorer17*, University of Western Australia, 2017, http://hirshfeldsurface.net.
54 C. J. O'Connor, *Prog. Inorg. Chem.*, 1982, **29**, 203.
55 D. F. Evans, *J. Chem. Soc.*, 1959, 2003; E. M. Schubert, *J. Chem. Educ.*, 1992, **69**, 62.
56 B. García and J. C. Ortega, *J. Chem. Eng. Data*, 1988, **33**, 200.